AD-A055 280 TEXAS INSTRUMENTS INC DALLAS CENTRAL RESEARCH LABS F/G 9/5
DEVELOPMENT OF CIRCUIT MODELS FOR SAW RESONATORS.(U)
MAR 78 W R SHREVE, R S WAGERS N00173-77-C-0006
UNCLASSIFIED TI-08-78-07 NL

1 OF 1
AD
A055 280

END
DATE FILMED
7-78
DDC

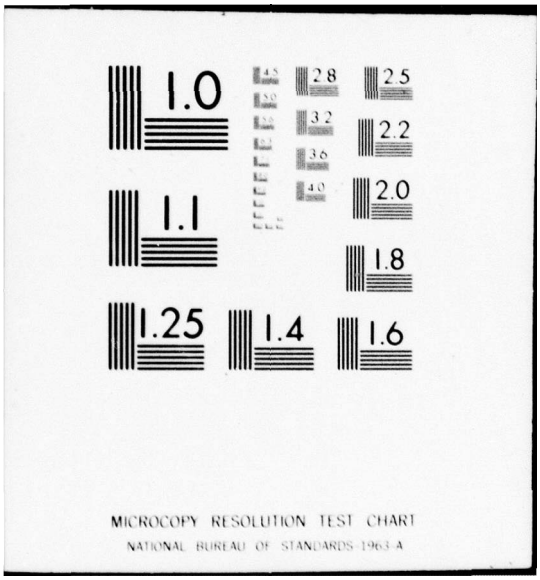
1.0
1.1
1.25
1.4
1.6
1.8
2.0
2.2
2.5
2.8
3.2
3.6
4.0
MICROCOPY RESOLUTION TEST CHART
NATIONAL BUREAU OF STANDARDS 1963-A

DEVELOPMENT OF CIRCUIT MODELS FOR SAW RESONATORS

William R. Shreve
Robert S. Wagers

Texas Instruments Incorporated
Central Research Laboratories
13500 North Central Expressway
Dallas, Texas 75222

March 1978

Final Technical Report for Period 29 October 1976 - 31 January 1978

Prepared for

Naval Research Laboratory
4555 Overlook Avenue, S. W.
Washington, D. C. 20375

UNCLASSIFIED

SECURITY CLASSIFICATION OF THIS PAGE (When Data Entered)

REPORT DOCUMENTATION PAGE	READ INSTRUCTIONS BEFORE COMPLETING FORM
1. REPORT NUMBER	2. GOVT ACCESSION NO. / 3. RECIPIENT'S CATALOG NUMBER
4. TITLE (and Subtitle) DEVELOPMENT OF CIRCUIT MODELS FOR SAW RESONATORS.	5. TYPE OF REPORT & PERIOD COVERED Final Technical Report. 29 Oct 1976 - 31 Jan 1978
	6. PERFORMING ORG. REPORT NUMBER TI-08-78-07
7. AUTHOR(s) William R. Shreve, Robert S. Wagers	8. CONTRACT OR GRANT NUMBER(s) N00173-77-C-0006
9. PERFORMING ORGANIZATION NAME AND ADDRESS Texas Instruments Incorporated, Central Research Laboratories, 13500 North Central Expressway, Dallas, Texas 75222	10. PROGRAM ELEMENT, PROJECT, TASK AREA & WORK UNIT NUMBERS
11. CONTROLLING OFFICE NAME AND ADDRESS Naval Research Laboratory, 4555 Overlook Avenue, S. W., Washington, D. C. 20375	12. REPORT DATE March 1978
	13. NUMBER OF PAGES 22 (12) 26 p.
14. MONITORING AGENCY NAME & ADDRESS(if different from Controlling Office)	15. SECURITY CLASS. (of this report) Unclassified
	15a. DECLASSIFICATION/DOWNGRADING SCHEDULE

16. DISTRIBUTION STATEMENT (of this Report)

17. DISTRIBUTION STATEMENT (of the abstract entered in Block 20, if different from Report)

18. SUPPLEMENTARY NOTES

19. KEY WORDS (Continue on reverse side if necessary and identify by block number)

20. ABSTRACT (Continue on reverse side if necessary and identify by block number)

Three approaches for calculating the surface acoustic wave (SAW) velocity in the periodic reflector array of a SAW resonator have been undertaken. A theoretical model of the velocity in the array could be used to improve existing resonator models and thus to improve device performance. All three approaches involve approximate theoretical calculations. The first two approaches--a variational method and a perturbation theory--were not sufficiently accurate in

DD FORM 1 JAN 73 1473 EDITION OF 1 NOV 65 IS OBSOLETE

403 833

UNCLASSIFIED

SECURITY CLASSIFICATION OF THIS PAGE (When Data Entered)

their simplest implementation. More accurate field approximations than those previously available are needed to give the required accuracy. A finite element calculation aimed at obtaining better field estimates has been completed. The only step remaining when the contract terminated was the utilization of the more accurate field approximations obtained by the finite element method in an improved perturbation calculation.

TABLE OF CONTENTS

LIST OF TABLES

LIST OF ILLUSTRATIONS

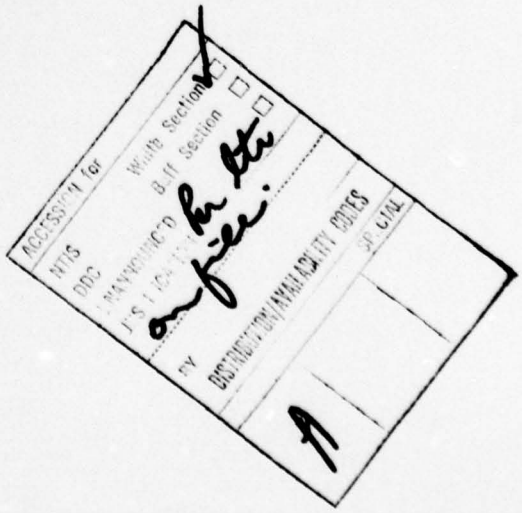

SECTION I
INTRODUCTION

The purpose of this program is to study wave propagation in anisotropic periodic media and generate a theory based on fundamental physical principles that will lead to models to replace current materials-specific ad hoc models for surface acoustic wave resonators. The goals of the program are improved modeling of resonators, improved device performance, and increased capability to analyze new materials combinations.

This report describes three approaches used to predict the primary reflector array property not included in current basic models, the shift in velocity under the reflector array. This shift is observed as a change in the frequency of maximum reflection of the array as the size of the reflector perturbation is varied. An understanding of this phenomenon should lead to a fundamental model similar to the ad hoc stored energy model proposed by R. C. M. Li and J. Melngailis.[1] The first two approaches used were a variational calculation and a perturbation analysis. Neither yielded results that agreed with experiments, primarily because the field approximations used were not sufficiently accurate. A finite element calculation aimed at obtaining better field estimates has been completed. This analysis yields approximate velocities and the displacement fields within the substrate. The only step remaining when the contract terminated was linking the displacement field from the finite element analysis to the stress fields used in the perturbation analysis.

---

1. R. C. M. Li and J. Melngailis, "The Influence of Stored Energy at Step Discontinuities on the Behavior of Surface Wave Gratings," IEEE Trans. Sonics Ultrason. SU-22, 189 (1975).

SECTION II
VARIATIONAL CALCULATION

The purpose of this analysis is to determine the shift in velocity under an array of reflectors in terms of the specific substrate-reflector combination chosen for the resonator. The type of shift considered has been detected experimentally by measuring the change in frequency of maximum reflection of an array of grooves as a function of groove depth. This variation has not been predicted by any existing fundamental theory.

The problem was approached as a waveguide-type problem. Piezoelectricity and anisotropy of the substrate are included. The system considered is shown in Figure 1. Waveguide problems of this type have been treated by considering the wave number β as an independent variable and using resonator-type variational expressions for frequency ω. In this, β is fixed by the geometry of the structure. Therefore, an expression for $\omega = v\beta$ will give a direct determination of the effective velocity v under the array. The fixed value of β in the array is similar to the fixed β determined by the boundaries of a bulk resonator. The allowable β determines the normal modes of oscillation of the resonator.

A variational expression for the oscillator frequency of a nonpiezoelectric resonator has been derived by Auld.[2] The advantage of using a variational expression stems from its stationary property; the value obtained by using an approximate or trial solution in the expression has only a second-order error relative to the error in the trial solution. If a derivation identical to that used by Auld to obtain Equation (13-3) is used for a piezoelectric substrate, one obtains the following:

$$\omega^2 = \frac{\int_V \nabla_s v : \left[c : \nabla_s v + e \nabla \frac{\partial \phi}{\partial t} \right] dV - \int_S v \cdot \left[c : \nabla_s v + e : \nabla \frac{\partial \phi}{\partial t} \right] \cdot \hat{n} \, dS}{\rho \int_V v \cdot v \, dV} \quad . \quad (1)$$

2. B. A. Auld, Acoustic Fields and Waves in Solids, Vol. II (John Wiley & Sons, Inc., New York, 1973).

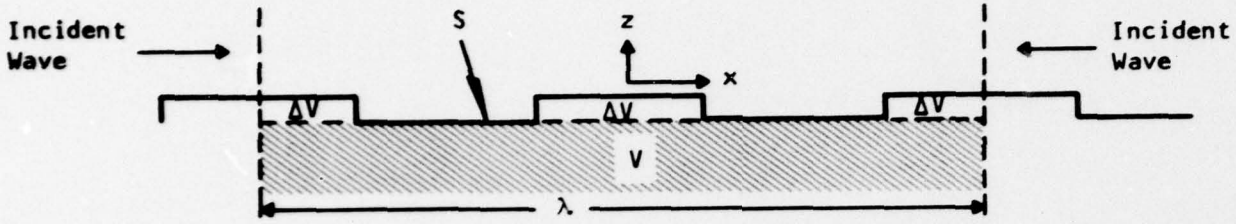

Figure 1 Geometry of Structure Analyzed in Variational Calculation

The notation is the same as that used by Auld:

∇_s is the symmetric gradient operator,

v is the particle velocity,

e is the piezoelectric stress matrix,

ϕ is the electric potential,

c is the permittivity matrix, and

$\hat{n}$ is the surface normal.

In the analysis of the SAW resonator reflector, the fields used in this expression correspond to an unperturbed Rayleigh wave and a third space harmonic. The fundamental Rayleigh wave satisfies the equations of motion on an unperturbed half-space. The third harmonic satisfies the same equations when driven by a source at the bottom of the groove. The relative amplitudes were chosen so that the total normal stress at the bottom of the groove was as small as possible. Equal amplitude waves were assumed to be incident from the two sides of the section considered so that reflection effects would cancel in the integrals. The medium was assumed to be lossless.

The integrals in the numerator of Equation (1) were divided into parts so that the significant contributions to the frequency could be determined. The volume integral was split into two parts, one covering the half-space V and the other covering the pedestal ΔV. In ΔV the contributions of the third-harmonic fields were ignored. Since the volume here is small and the fields are a small part of the acoustic disturbance, this approximation should be valid. In V both sets of fields were considered. The surface integral was divided into contributions from the fundamental Rayleigh mode and contributions from the third harmonic.

The results of this velocity calculation as a function of groove depth are shown in Table 1. The columns represent the velocity shift caused by different terms in the integrals and different integrals in the numerator. One can see that the major contribution to the velocity shift is from the surface integral. Since this integral contains a normal stress, $T \cdot \hat{n}$, multiplicative term, it should vanish for the true fields. For a variational calculation like this to yield results to the desired accuracy, field approximations that more nearly satisfy the boundary condition are required; a more complete basis set is needed for the calculation.

The results obtained show that the net dependence on h/λ is approximately linear as opposed to the observed quadratic variation. It is also clear that the third-harmonic term does not have the expected effect of introducing a significant velocity shift.

The conclusion of this analysis is that more accurate basis fields are needed to obtain meaningful velocity shifts. All other results must be rechecked when these corrected fields are used.

Table 1

Velocity Shift (m/s) from 3487.77 m/s

Groove Depth h/λ	Experimental	Fundamental Fields Only			Third Harmonic Fields Included		
		Integral 1	Integrals 1 & 2	Integrals 1, 2, & 3	Integral 1	Integrals 1 & 2	Integrals 1, 2, & 3
0	0.0	+0.1	+0.1	-0.3			
0.005	-1.2	-1.7	-4.3	-12.9			
0.010	-4.7	-2.1	-7.3	-24.1	-1.7	-6.8	-24.0
0.015	-10.5	-1.5	-9.2	-34.0			
0.020	-18.7	+0.3	-9.9	-42.6			
0.025	-29.1	+3.0	-9.7	-50.0			
0.030	-42.0	+6.5	-8.5	-56.3			

Integral 1 is the integral over the volume V

Integral 2 is the integral over the volume ΔV

Integral 3 is the integral over the surface S

SECTION III

PERTURBATION CALCULATION

To try to bypass the field-sensitive limitations of the variational calculation, a perturbation approach was pursued. The starting point for this calculation is Rayleigh wave propagation on an unperturbed half space. The frequency is fixed by selecting a Rayleigh wave length equal to twice the period of the perturbation. The shift in frequency generated by introducing perturbations on the surface is calculated directly. [In the variational calculation, the absolute velocity (or frequency) was calculated, leading to a larger margin for error.] The perturbation expression used is derived from the complex reciprocity relation, a general acoustic field theorem applicable to lossless media. This theorem is derived from the acoustic equations of motion by assuming two solutions to the field equations exist and each is driven by its own source terms. This derivation is given directly by Auld [Equation (10.113)].

$$\nabla\cdot\left(-v_2^{*}\cdot T_1 - v_1\cdot T_2^{*} + \phi_2^{*}\frac{\partial D_1}{\partial t} + \phi_1\frac{\partial D_2^{*}}{\partial t}\right) = -\frac{\partial}{\partial t}\left\{\left[v_2^{*}\ T_2^{*} - \nabla\phi_2^{*}\right]\cdot\begin{bmatrix}\rho & 0 & 0\\ 0 & s^{E} & d\\ 0 & d & \epsilon^{T}\end{bmatrix}\cdot\begin{bmatrix}v_1\\ T_1\\ -\nabla\phi_1\end{bmatrix}\right\} + v_2^{*}\cdot F_1 + v_1\cdot F_2^{*} + \phi_2^{*}\frac{\partial \rho_{e1}}{\partial t} + \phi_1\frac{\partial \rho_{e2}}{\partial t}$$

Assume the following:

Solution 1 is the solution for the perturbed system.

Solution 2 is the solution for the unperturbed half space.

Solution 1 varies as $e^{-j\omega_1 t}$.

Solution 2 varies as $e^{-j\omega_2 t}$.

No body forces ($F = 0$).

No time-dependent density ($\partial\rho/\partial t = 0$).

Integrate over the unperturbed half space, and the right side of the equation above becomes

$$-j(\omega_2 - \omega_1) \int_V [\rho\, v_1\, v_2^* + T_2^* : s : T_1 - T_2^* : d \cdot \nabla\phi_1 - \nabla\phi_2^* \cdot d : T_1 + \nabla\phi_2^* \cdot \varepsilon \cdot \nabla\phi_1]\, dV =$$

$$-j(\omega_2 - \omega_1) \int_V [\rho\, \omega_1\, \omega_2\, U_1\, U_2^* + S_2^* : c : S_1 + E_2^* \cdot \varepsilon^S \cdot E_1]\, dV \quad .$$

Application of the divergence theorem to the left side yields the result

$$\oint_S (-v_2^* \cdot T_1 - v_1 \cdot T_2^* - j\omega\phi_2^* D_1 + j\omega_2 \phi_1 D_2^*) \cdot \hat{n} dS.$$

Assuming there is no charge buildup in the material ($\rho = 0$) and the surfaces are stress-free ($T \cdot \hat{n} = 0$), only the first term contributes, and the integral becomes

$$-\oint_S v_2^* \cdot T_1 \cdot \hat{n} dS \quad .$$

Therefore, the overall expression can be solved for the fractional frequency shift

$$\Delta\omega = \frac{\oint_S v_2^* \cdot T_1 \cdot \hat{n} dS}{-j \int_V \rho\omega_1\omega_2 U_1 U_2^* + S_2^* : c : S_1 + E_2^* \cdot \varepsilon^S \cdot E_1\, dV} \quad .$$

One can simplify this expression by assuming that the surface perturbation will have only a small effect on the volume integral. This assumption allows one to use only the unperturbed "2" fields in the volume integral.

$$\Delta\omega = \frac{\oint_S v_2^* \cdot T_1 \cdot \hat{n} dS}{-j \int_V \rho\omega^2 |U|^2 + S_2^* : c : S_2 + E_2^* \cdot \varepsilon_S \cdot E_2\, dV} \quad . \qquad (2)$$

The problem has been reduced to a calculation of the component of the perturbed stress normal to the unperturbed surface $T_1 \cdot \hat{n}$.

As a special case, consider a surface with a sinusoidal perturbation of the surface like that shown in Figure 2. The surface is defined by the expression $z = f(x) = \frac{1}{2}(1 + \cos 2\pi x/p)h$. To evaluate $\Delta\omega$, one needs to know the component of the perturbed stress normal to the unperturbed surface ($z = 0$), $T_1(0)\cdot\hat{z}$, where $\hat{z}$ is a unit vector in the z direction. The perturbed surface is stress-free, so the boundary condition at this surface is $T_1[f(x)]\cdot\hat{z}' = 0$, where $\hat{z}'$ is the normal to the perturbed surface. If the surface perturbation is small ($f(x) \ll 1$) and the slope of the perturbed surface is small ($df/dx \ll 1$), then one can expand the perturbed stress $T_1(z)$ in a Taylor series about $z = f(x)$ and evaluate $T_1(0)\cdot\hat{z}$ to give the result

$$T_1(0)\cdot\hat{z} \cong T_1(f(x))\,\frac{df}{dx}\cdot\hat{x}' - f\left.\frac{dT_1}{dz}\right|_{z=f(x)}\cdot\hat{z}' - f\,\frac{df}{dx}\left.\frac{dT_1}{dz}\right|_{z=f(x)}\cdot\hat{x}' + \frac{f^2}{2}\left.\frac{d^2T_1}{dz^2}\right|_{z=f(x)}\cdot\hat{z}' \quad . \tag{3}$$

For small perturbations, the tangential stress on the perturbed surface can be approximated by the tangential stress of an unperturbed Rayleigh wave on an unperturbed half space;

$$T_1(f(x))\cdot\hat{x}' \cong T_2(0)\cdot\hat{x} \quad . \tag{4}$$

Similarly,

$$\left.\frac{dT_1}{dz}\right|_{z=f(x)}\cdot\hat{x}' \cong \left.\frac{dT_2}{dz}\right|_{z=0}\cdot\hat{x} \quad , \tag{5}$$

and

$$\left.\frac{d^2T_1}{dz^2}\right|_{z=f(x)}\cdot\hat{z}' \cong \left.\frac{d^2T_2}{dz^2}\right|_{z=0}\cdot\hat{z} \quad . \tag{6}$$

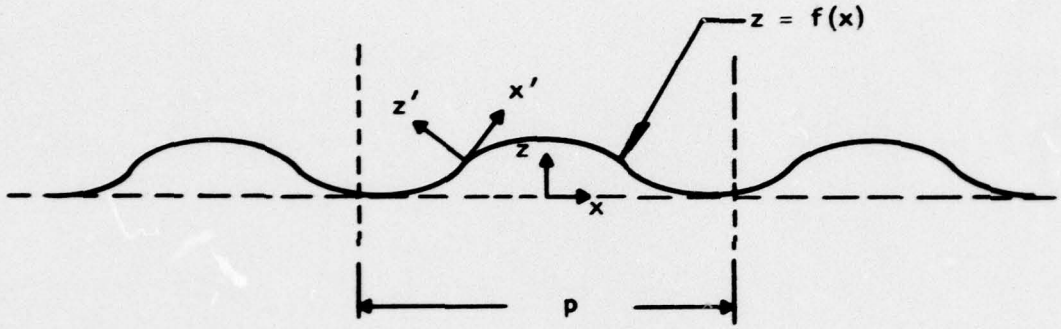

Figure 2 Perturbed Surface Showing Primed Coordinate System for Perturbation Calculation

These approximations are equivalent to assuming that for small perturbations the major change in the stress is caused by the change in the direction of the surface normal. This assumption should be good as long as df/dx is small. This is true for perturbations like the sinusoidal perturbation. As df/dx increases, arguments about normal and tangential stress and stress derivations being equivalent at perturbed and unperturbed surfaces break down.

The rectangular groove profile commonly used for reflector arrays can be expanded in a Fourier series. The first term of this series can be substituted for the sinusoidal perturbation f(x) in this analysis. Neglecting the other terms in the expansion, Equations (2) through (6) can be combined to predict the dependence of frequency on groove depth. This approximation results in the dependence shown by the dotted curve in Figure 3.

An expansion similar to that of Equation (3) can be carried out for trapezoidal grooves like those shown on the inset of Figure 3. This expansion can be carried out without the restriction $df/dx \ll 1$. For sloping grooves the results are the same as those for the sinusoidal perturbation. For steep grooves the results change to those shown by the solid line in Figure 3, but the approximations for the perturbed stress on the edges of these grooves [Equations (4), (5), and (6)] are not good. This fact explains the deviation from the experimental results shown in Figure 3. A better approximation to the perturbed fields is needed. The similarity of the experimental results to the steep groove theory is indicative of the fact that extremely accurate field approximations are not needed, since the field approximations used here are quite crude.

The finite element calculation described in the next section was intended to yield the improved field approximations needed for the surface integral in Equation (2).

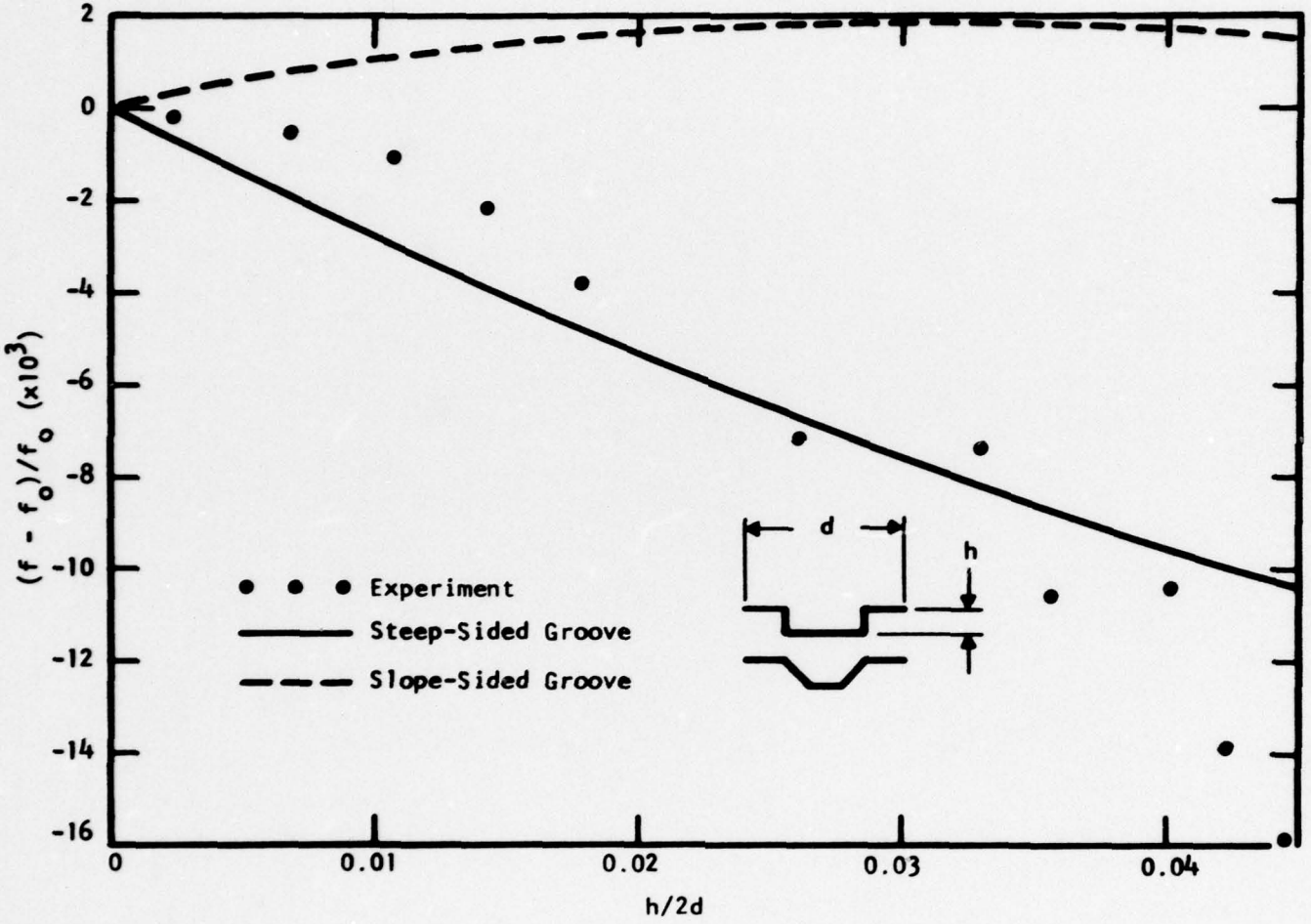

Figure 3 Dependence of Frequency on Groove Depth as Predicted by Perturbation Analysis

SECTION IV
FINITE ELEMENT CALCULATION

A. Introduction

The purpose of this calculation is to obtain an estimate of the field distribution in the substrate when it is perturbed by the presence of an array of reflectors. The starting point is the same as that of the variational calculation, Equation (1). In principle, this expression, when solved exactly, will predict the actual velocity perturbation. A finite element solution aimed at achieving the accuracy required to model the velocity shift caused by distributed arrays of weak reflectors leads to a calculation involving a large number of small elements. This approach involves prohibitively large numerical arrays and exceeds the capacity of modern computers.

The approach used here does not require this high degree of accuracy in the finite element calculation. The system is divided into a small number of large elements to keep the size of the numerical arrays within reasonable limits. This leads to a first-order approximation to the solution of Equation (1) in the substrate-reflector system. This approximate solution can be used to evaluate the stress T_1 in this system and to evaluate the numerator of the perturbation calculation expression, Equation (2). This perturbation calculation yields the accuracy required to model the weak perturbation.

Since the finite element calculation is designed to give only a first-order approximation to the field distribution, the effects of piezoelectricity will be ignored to simplify the calculation. From the fact that the stored energy velocity changes are nearly the same for grooves in ST quartz (a weak piezoelectric) and for grooves in YZ $LiNbO_3$ (a strong piezoelectric), one can conclude the effect is primarily mechanical and ignoring piezoelectricity is justified. This approximation and a rearrangement of terms reduces Equation (1) to the following:

$$\int_V \nabla_s \, v : c : \nabla_s v - \omega^2 \rho \int_V v \cdot v \, dV = 0. \qquad (7)$$

The surface integral vanishes in this analysis, since the normal stress is constrained to vanish in the calculation.

The displacement in the system is the unknown that we want to evaluate. The system is divided into rectangular cells. The displacement is expanded in terms of the position within the cell. Specific positions within each cell and on the boundaries between cells are selected as points where Equation (1) will be exactly satisfied. These positions are the nodes of the system. The displacement expansion coefficients can be evaluated in terms of the nodal displacements so that ultimately, the displacement at any point can be expressed in terms of the nodal displacements and the position within the cell. Equation (1) becomes an equation involving products of nodal displacements. The first term in the equation is the potential energy. The second term is the kinetic energy. Thus, the right side of the equation is the Lagrangian for the system. The derivative of the Lagrangian with respect to the nodal displacements vanishes identically, so the system of equations represented by Equation (1) reduces to a system of linear simultaneous equations. For this system to have a nontrivial solution, the determinant of the coefficients must vanish. This condition fixes the perturbed system velocity. The relative displacements of the nodes can then be found by solving the system of equations.

B. Approach

This section contains the details of the finite element calculation. The governing equations and manipulations are detailed and their relation to the computer calculation is pointed out.

The starting point is an expansion of the displacement vector for use in Equation (7). All quantities in the analysis are assumed to vary as $e^{-j\omega t}$ so

that the particle velocity in Equation (7) can be expressed in terms of the displacement u.

$$v = -j\omega u \ .$$

In addition, we assume that there is no variation in the plane of propagation perpendicular to the direction of propagation; the acoustic beam is infinitely wide. The displacement is expanded in terms of the position within the cell. The coordinate positions are expressed as a vector P and the coefficients are expressed as a matrix A.

$$u = A \cdot P \ . \tag{8}$$

The order of the polynomial P determines the order of the calculation. If P is a first-order polynomial,

$$P = [1,x,z] \ , \tag{9}$$

then the calculation is first-order. The true displacements are approximated by linear variations within each cell. When a large number of cells is used, a reasonably good approximation to the displacement is obtained. The order of P leads to two conditions on the nodes in the cell. First, to generate a system with an equal number of unknowns and equations, the number of nodes in each cell must equal the number of terms in P. Second, to guarantee that the displacement is continuous across cell boundaries, i.e., that the displacement along a cell wall is the same when evaluated from either of two adjacent cells, the order of the polynomial must be one less than the number of nodes along each side. The first condition establishes a one-to-one correspondence between the unknown coefficients A in Equation (8) and the nodal displacements that will become the unknowns in this analysis. The basis for the second condition is the uniqueness of the expansion of u along the boundary when the values of u are fixed at the nodes. These conditions are discussed in more detail by Zienkiewicz.[3]

3. O. C. Zienkiewicz, The Finite Element Method in Engineering Science (New York, McGraw Hill Book Co., 1971).

Consider first-order calculations as an example of satisifying these two conditions. The second condition states there must be two nodes on each side of the cell or, equivalently, one at each corner as shown in Figure 4. The first condition requires the number of terms in P to equal the total number of nodes in the cell. Thus, the triangular cell with three nodes [Figure 4(a)] is appropriate for a three-term polynomial like that in Equation (9). The structures of interest here divide naturally into rectangles. The cell in Figure 4(b) satisifies the continuity requirement, two nodes on each side, and matches a four-term polynomial. The appropriate polynomial for this case is

$$P = [1, x, z, xz] \quad .$$

Along any boundary one parameter, x or z, is fixed. Therefore, along that line the polynomial P has only two independent terms, and the coefficients of these terms are determined uniquely by the displacements at the two corner nodes.

Zienkiewicz states that greater accuracy can be achieved in a computation for a given number of nodes by increasing the order of P and therefore the number of nodes in a cell than by reducing the size of each cell and increasing the number of cells. Therefore, all calculations up to fourth-order were considered in this analysis. The polynomial used is as follows:

$$P = [1, x, z, xz, x^2, z^2, x^2z, xz^2, x^3, z^3, x^3z, x^2z^2, xz^3, x^4, z^4, x^4z, xz^4] \quad ,$$

where the first 4 terms are used for first-order, 8 for second, 13 for third, and all 17 for fourth-order calculations. The corresponding cells are shown in Figures 4(b) and 5.

Once the order of calculation and nodal positions have been chosen, the nodal displacements, u_n, can be evaluated in terms of the coefficients A in

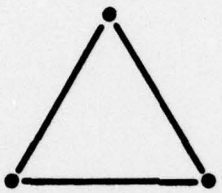

(a)

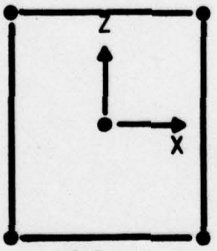

(b)

Figure 4 Cells for First-Order Finite Element Calculations

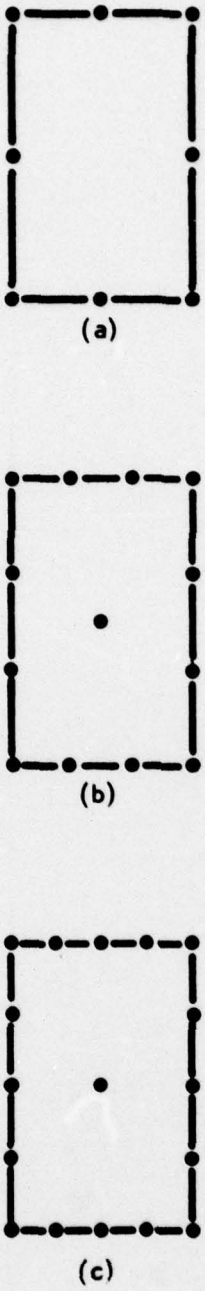

Figure 5 Cells for Finite Element Calculations. (a) Second-order, (b) third-order, (c) fourth-order.

Equation (8) by evaluating P at the node positions. To express this in matrix form, let N be number of nodes and u_n be a 3 by N element matrix (one element for displacement along each axis at each node); then A must be a matrix with 3 by N elements and the nodal polynomial matrix Q is an N by N matrix formed by evaluating P at the nodes.

$$u_n = A \cdot Q \quad .$$

This expression can be inverted, since Q is a known matrix:

$$A = u_n \cdot Q^{-1} \quad .$$

Combining this expression with Equation (8) gives the following expression for the displacement at any point within a cell in terms of the displacement at the nodes:

$$u = u_n \cdot Q^{-1} \cdot P \quad . \tag{10}$$

This expression can be used in Equation (7) for the displacement in this cell, but Equation (7) applies only to the system as a whole, not to individual cells. Thus, the contributions to the volume integrals from each cell must be summed to give the desired system of equations.

$$\sum_{\substack{\text{all} \\ \text{cells}}} \left\{ \int_{V_c} \nabla_s \, u : c : \nabla_s \, u \, dV - \omega^2 \rho \int_{V_c} u \cdot u \, dV \right\} = 0 \quad . \tag{11}$$

where V_c is the particular cell volume. When Equation (10) is used for the displacement in Equation (11), the displacements u_n can be removed from the integrals, and the integrals can be evaluated analytically. This results in a system of $3 \cdot N_o$ quadratic equations in the nodal displacement, where N_o is the total number of nodes in the system. Since the left side of Equation (11) is the Lagrangian for the system, its derivative with respect to each nodal displacement must vanish. This differentiation results in a system of $3 \cdot N_o$ homogeneous equations in $3 \cdot N_o$ unknowns of the following form:

$$\left[PE - \left(\frac{v_p}{v_o} \right)^2 KE \right] u_n = 0 \quad . \tag{12}$$

where PE and KE are matrices made up of the contributions from all cells to the integrals in Equation (11). The phase velocity of the wave in the system being analyzed is v_p and the unperturbed substrate velocity is v_o, an input parameter. For these equations to have a nontrivial solution, the determinant of the coefficient matrix must vanish. This condition sets the value for the ratio v_p/v_o. The value is determined numerically with a zero crossing subroutine.

This portion of the analysis routine was checked by analyzing an ST quartz substrate. For this case the correct value for the velocity ratio is 1.0. The system analyzed was a two-wavelength thick substrate with the top surface free and the bottom surface rigid. The ratio was found to be 0.96 ± 0.01. Increasing the thickness of the slice from 3 wavelengths to 3.5 wavelengths increased the ratio to 1.00 ± 0.01. This answer verified the validity of the approach, and the analysis proceeded. (The accuracy was not adequate to bypass the perturbation analysis.)

The next quantities of interest are the nodal displacements themselves. The system of equations represented by Equation (12) is degenerate once the value of v_p/v_o is determined. Discarding one equation and using the corresponding displacement as a reference, the relative displacements of the nodes can be determined. Equation (12) reduces to the following:

$$\text{Lag} \cdot u_n' = b \quad , \tag{13}$$

where Lag is the same as the square matrix in Equation (12) with one row and one column removed, u_n' is the displacement matrix normalized to the reference displacement, and b is a column vector of constants formed from the column that was removed from Equation (12) to form the matrix Lag. This set of equations is the same as the set in Equation (12) with one displacement set to unity and the corresponding equation removed.

Inverting the matrix Lag in Equation (13) gives the nodal displacements, which can be used in Equation (10) to obtain expressions for the displacements in each cell of the system.

The finite element method has been used to obtain approximate solutions for the velocity and displacement fields in a propagation medium of arbitrary cross section. From the displacement field, one can calculate the stress field required for the perturbation analysis described in Section II of this report. The perturbation calculation will yield an accurate value for the change in velocity caused by the reflector array.

This approach creates a basis for determining the variation of SAW velocity in a reflector array consisting of arbitrary reflector-substrate material combinations. For example, the dependence of the velocity in an array of grooves on groove depth can be determined. Similarly, the velocity changes caused by an array of metal stripes forming a reflector or transducer can be determined. The steps remaining to connect the two sections of this work are conceptually straightforward, but were not completed during the contract period.

From the accurate velocity perturbation one can also create a transmission line model for propagation in the periodic array that is based on fundamental principles. This may simply consist of postulating a more complex form for the variation of the storage term, B, in the Li and Melngailis[4] stored energy model for the array that will extend its application to deep grooves.

The remaining goals of the contract -- to study dispersion of Rayleigh waves and scattering at oblique angles in an infinitely wide grating array -- were not pursued in this work. The approach that would have been used to achieve these goals was dependent on the results of the velocity calculation and could not be fruitfully pursued in a parallel analysis.

4. R. C. M. Li and J. Melngailis, op. cit.

SECTION V
SUMMARY

Three approaches have been used to predict the shift in velocity under an array of identical reflectors as the reflection coefficient per reflector is varied. A variational calculation was tried and found to be too sensitive to the basis functions available as initial guesses. A perturbation analysis was found to give better results, but again failed to give reliable agreement because of limitations in the ability of field expansions to model the rapid stress variations at reflector edges. Finally, a finite element solution of the equations of motion was used to obtain more accurate approximations to the field distributions needed for the perturbation analysis. The interface between the finite element and perturbation calculations is incomplete at present. Completion of this interface will allow one to predict the variation of velocity under a reflector array.